Electronic Supplementary Information for

A High-Temperature Performing and Near-Zero Energy Loss Lead-Free Ceramic Capacitor

Da Li, Diming Xu, Weichen Zhao, Max Avdeev, Hongmei Jing, Yan Guo, Tao Zhou, Wenfeng Liu, Dong Wang, Di Zhou

* Corresponding Author.

E-mail addresses: diming.xu@xjtu.edu.cn (Diming Xu)

wang_dong1223@mail.xjtu.edu.cn (Dong Wang)

zhoudi1220@gmail.com (Di Zhou)

This PDF file includes:

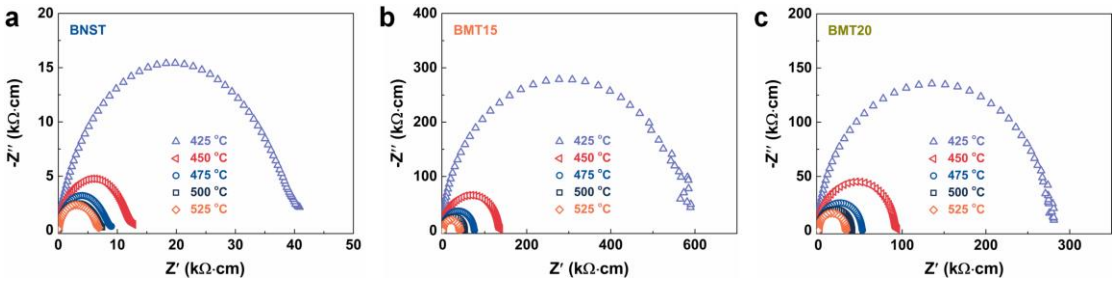

Fig. S1 Z^* plots at various temperatures for (a) BNST, (b) BMT15 and (c) BMT20 ceramics.

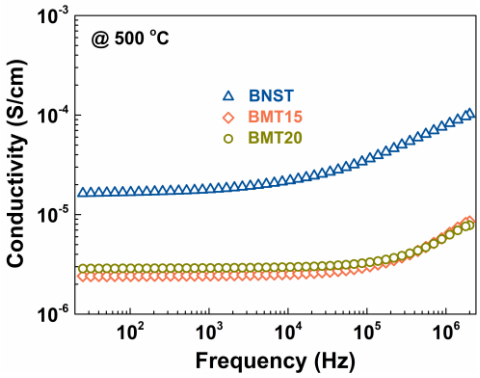

Fig. S2 Conductivity as a function of frequency measured at 500 °C for (1-*x*)BNST-*x*BMT ceramics.

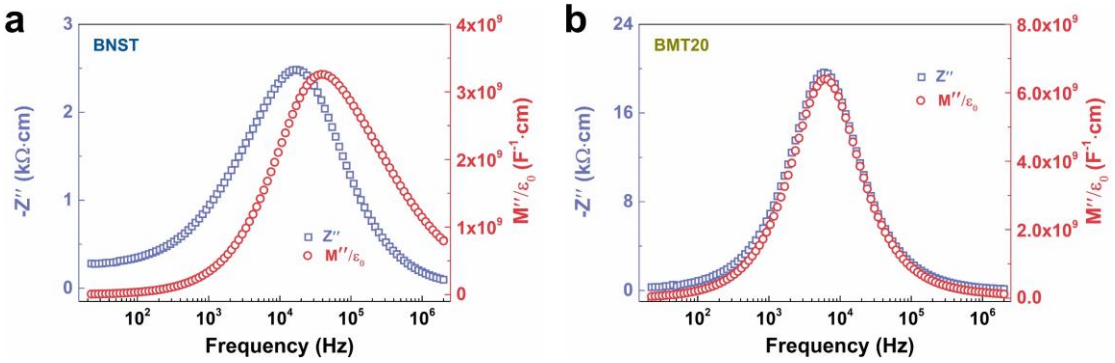

Fig. S3 Spectroscopic plots of Z″ and M″ spectra at 500 °C for (a) BNST and (b) BMT20 ceramics.

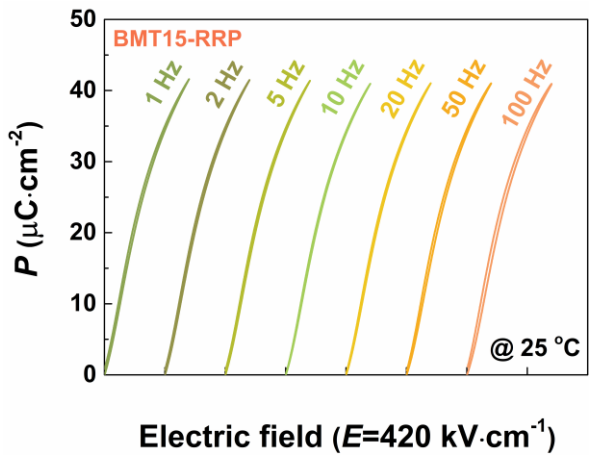

Fig. S4 Frequency-dependent *P*-*E* loops at 420 kV·cm^{-1} for the BMT15-RRP ceramic.

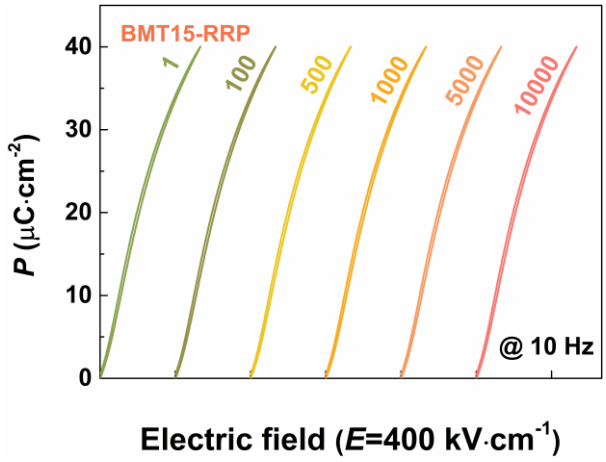

Fig. S5 Unipolar *P*-*E* loops for BMT15-RRP ceramic at 400 kV·cm^{-1} under various cycle numbers.

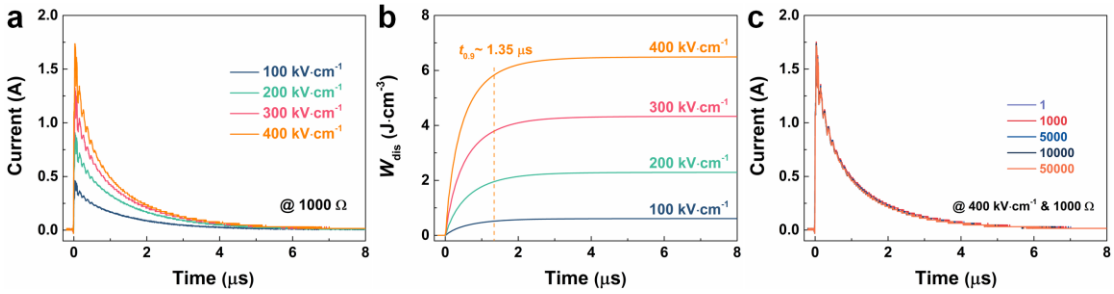

Fig. S6 (a) Overdamped discharge waveforms and (b) time-dependent discharge energy density (W_{dis}) under different electric fields. (c) Current curves as a function of the cycle number at room temperature of BMT15-RRP ceramics, measured by an RC load circuit.

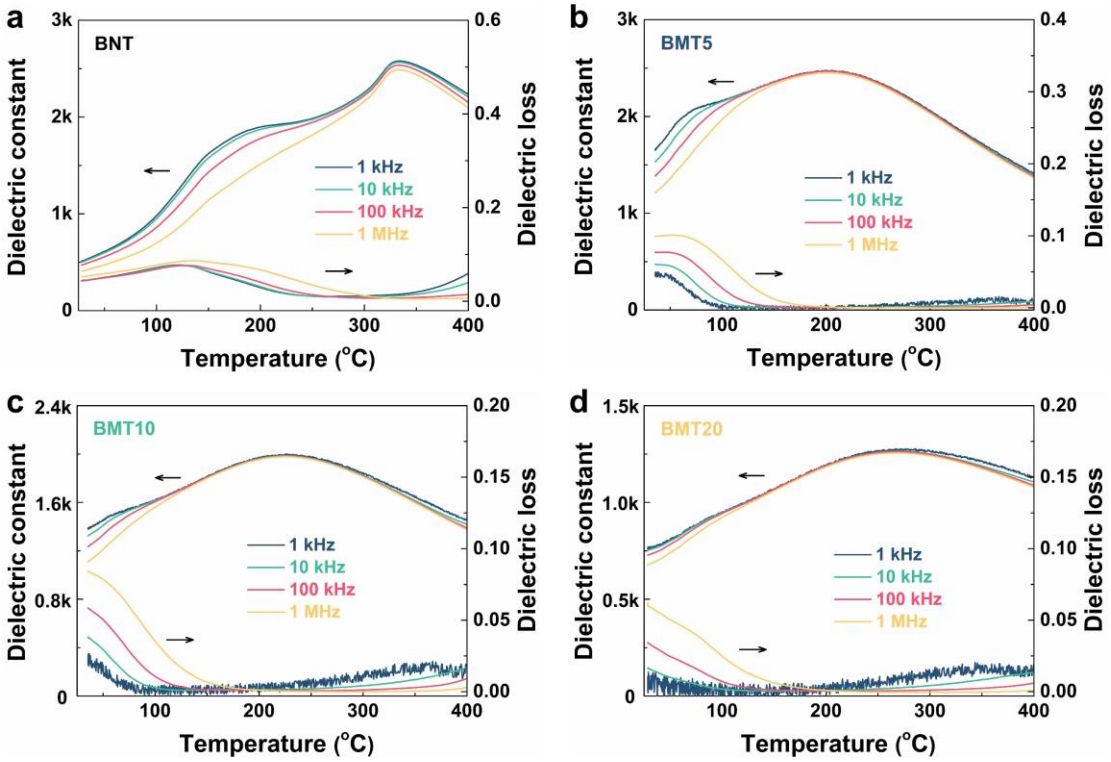

Fig. S7 Dielectric constant and dielectric loss as a function of temperature at various frequencies for (a) BNT, (b) BMT5, (c) BMT10 and (d) BMT20.

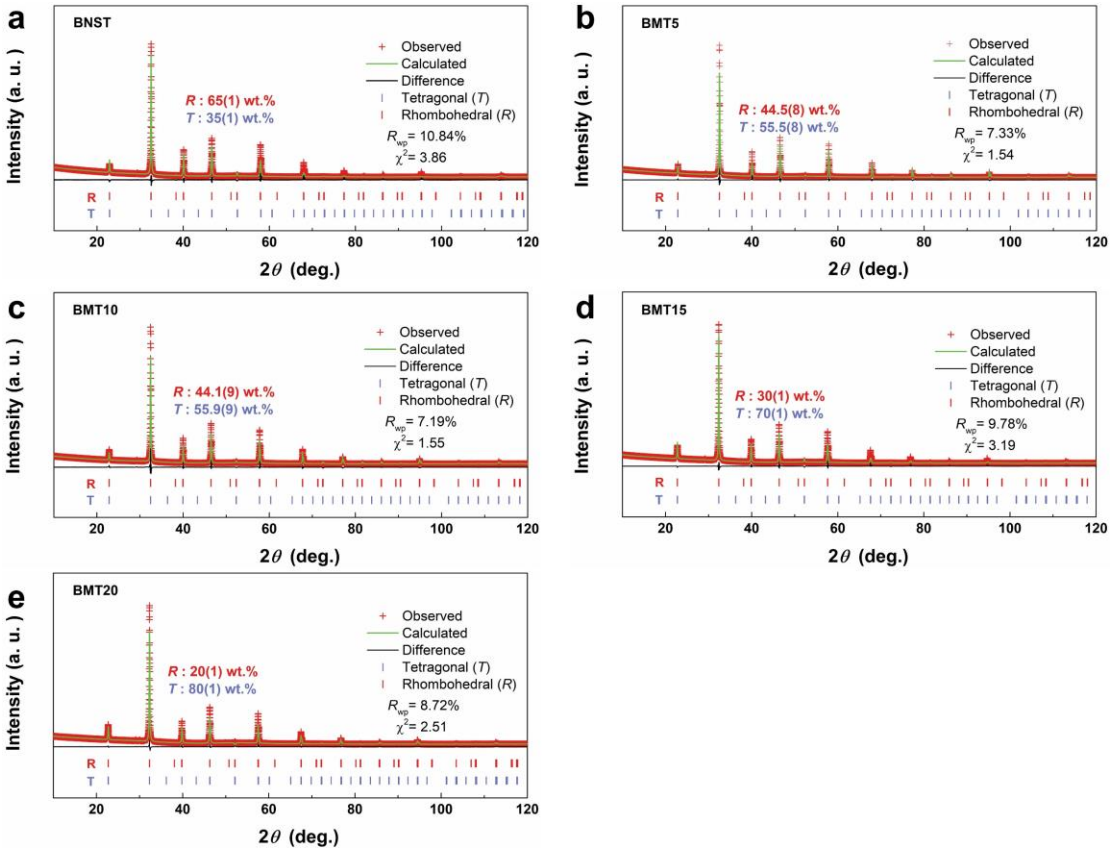

Fig. S8 The Rietveld refinement of XRD data for the (a) BNST, (b) BMT5, (c) BMT10, (d) BMT15 and (e) BMT20 ceramics.

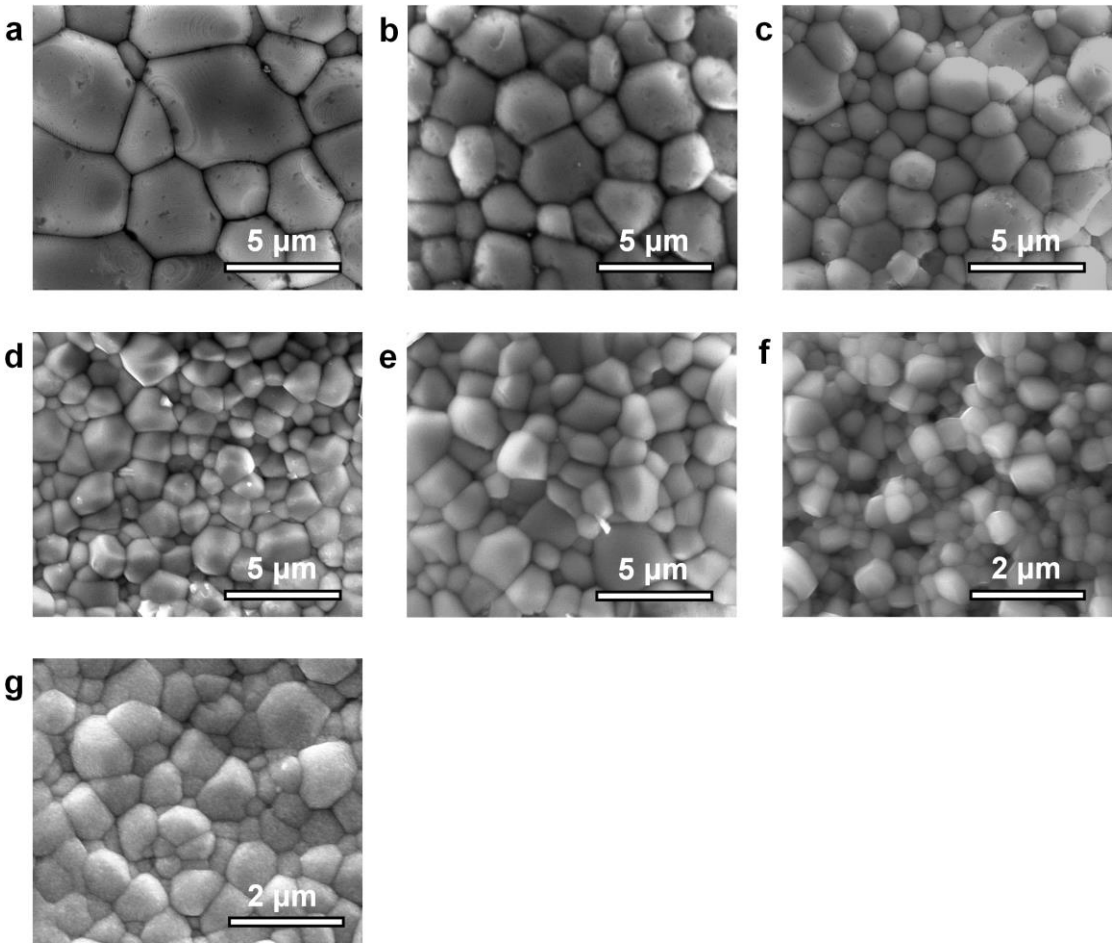

Fig. S9 SEM micrographs of BNST-BMT ceramics. (a) BNST, (b) BMT5, (c) BMT10, (d) BMT15, (e) BMT20, (f) BMT15-RRP and (g) BMT20-RRP.

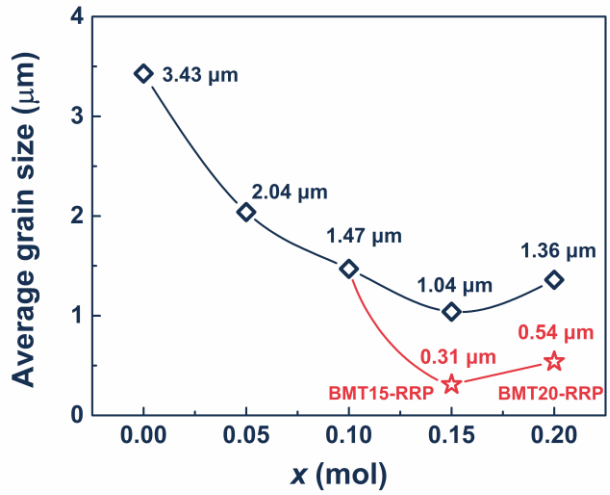

Fig. S10 Evolution of average grain size of the BNST-BMT ceramics.

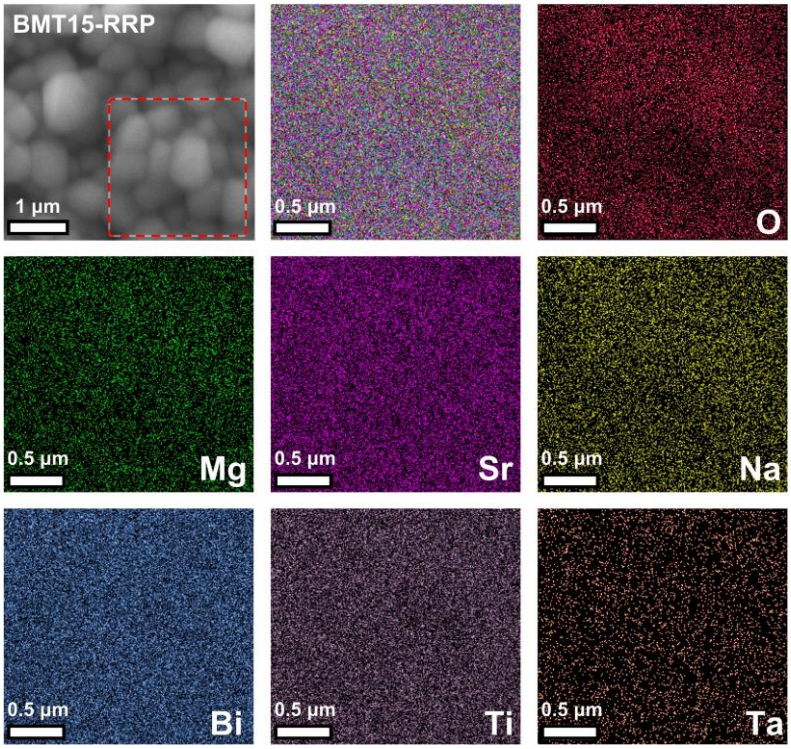

Fig. S11 SEM micrograph of BMT15-RRP ceramic and its corresponding EDX element mapping. Red-O, Green-Mg Purple-Sr, Yellow-Na, Blue-Bi, Gray-Ti and Orange-Ta.

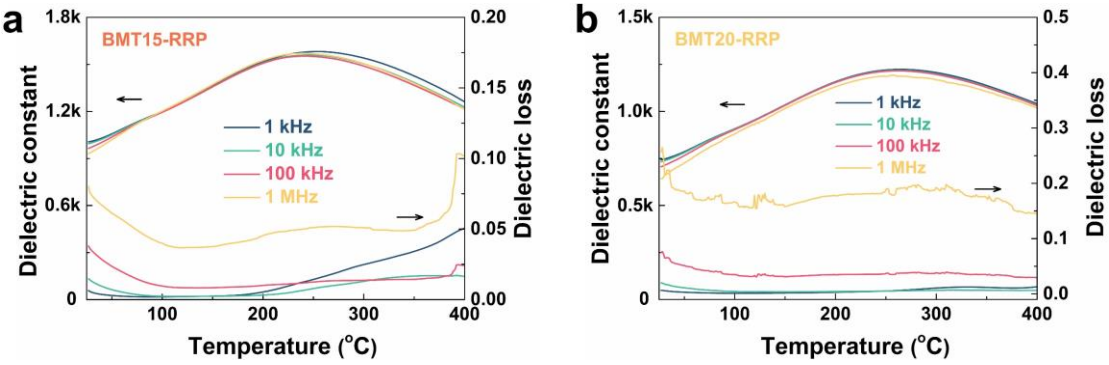

Fig. S12 Dielectric constant and dielectric loss as a function of temperature at various frequencies for (a) BMT15-RRP and (b) BMT20-RRP ceramics.

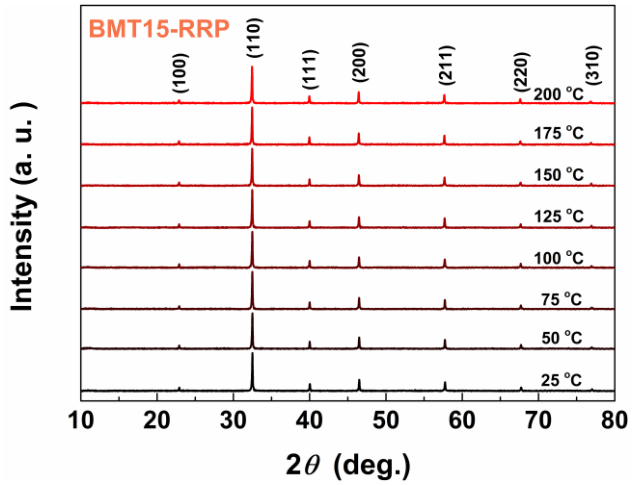

Fig. S13 Temperature-dependent XRD of BMT15-RRP ceramic.

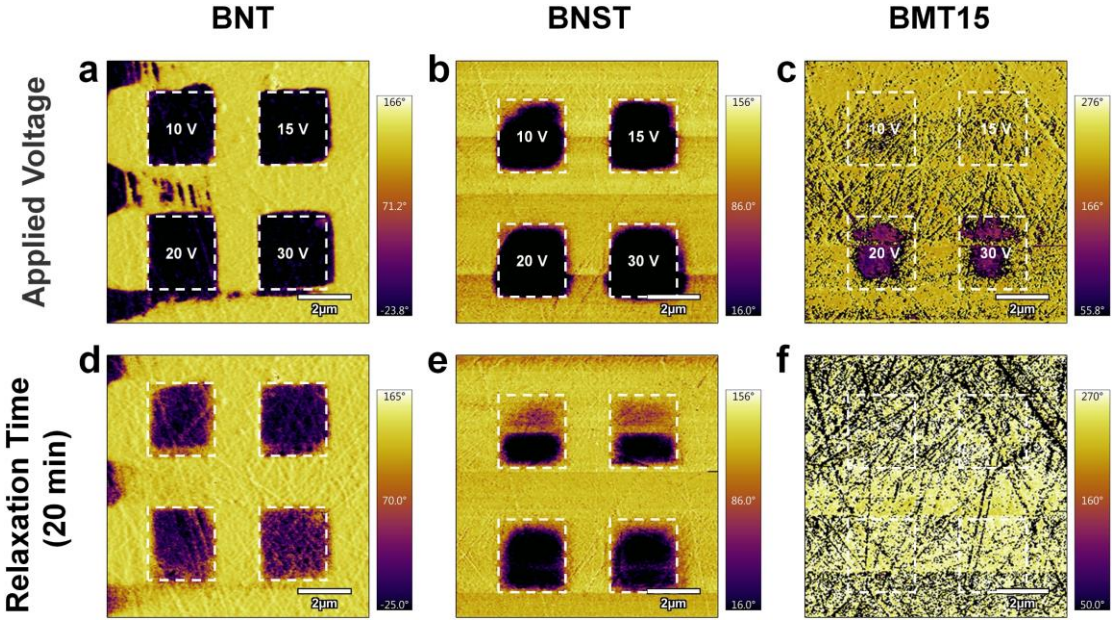

Fig. S14 Out-of-plane PFM phase images after poling treatment with different electrical voltages and relaxation durations. (a, d) BNT, (b, e) BNST and (c, f) BMT15.

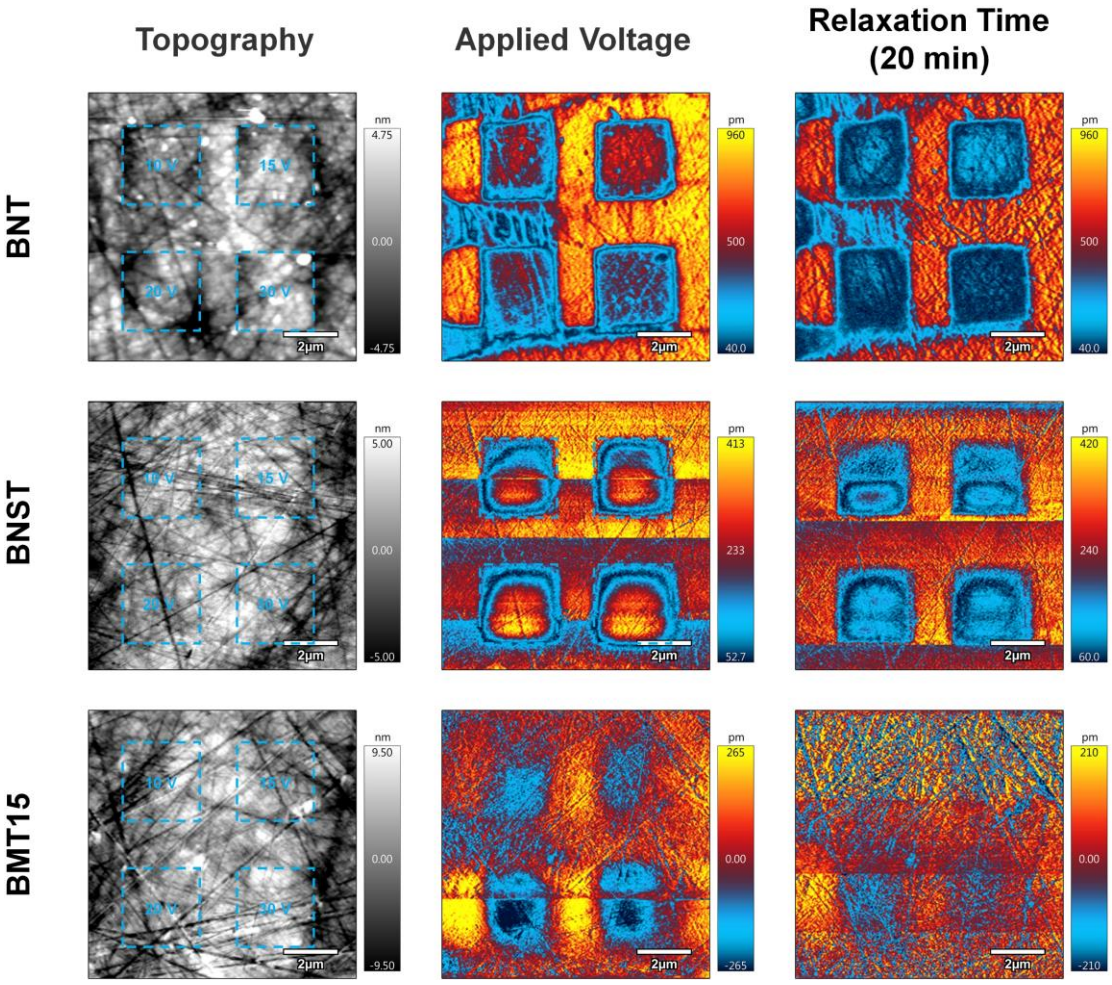

Fig. S15 Out-of-plane PFM amplitude images of the BNST-BMT ceramics after poling treatment with different voltages and relaxation durations.

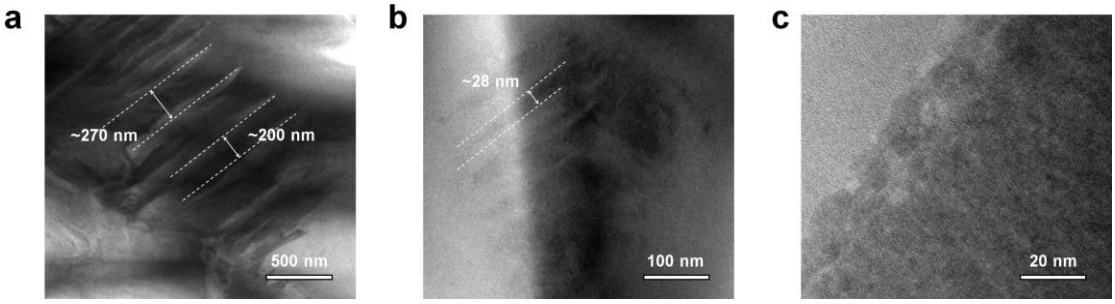

Fig. S16 Coexistence of polymorphic polar nanoregions. HR-TEM micrographs of (a) BNT, (b) BNST and (c) BMT15 ceramics.

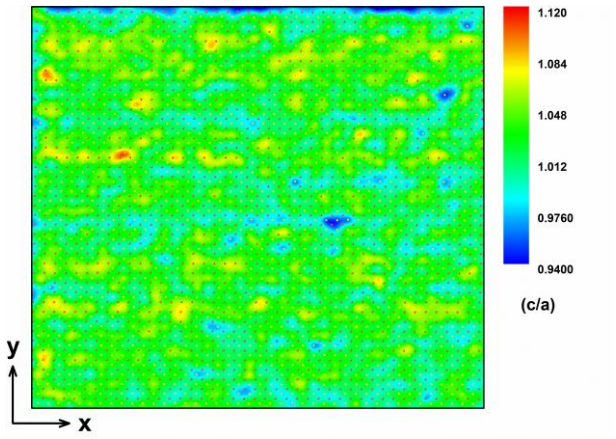

Fig. S17 Axial ratio (c/a) distribution mapping along $[100]_c$.

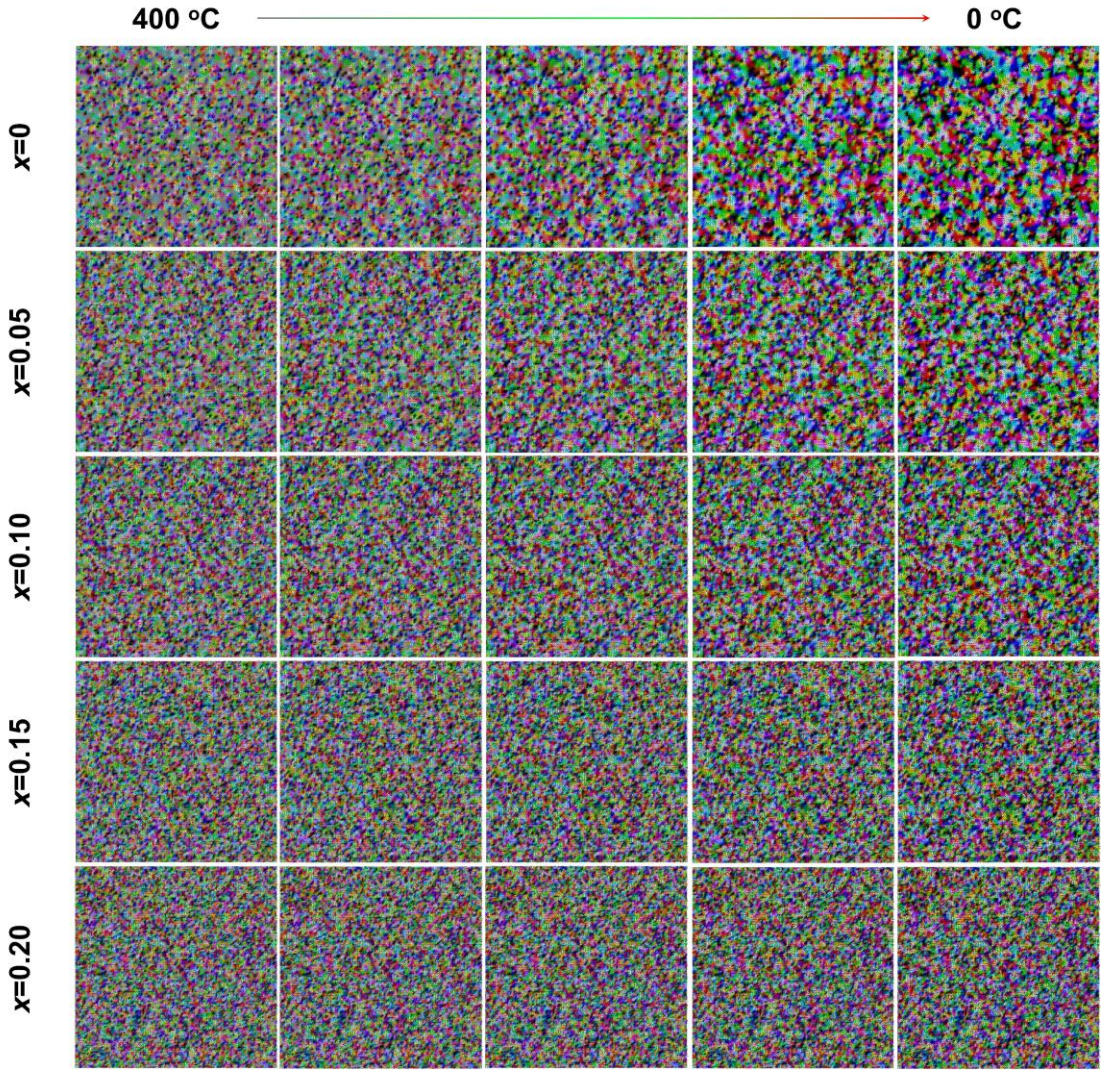

Fig. S18 Calculated microstructural evolution of (1-x)BNST-xBMT system upon cooling. The gray color represents the paraelectric phase, the other colors distinguish the ferroelectric domains with different orientations (arrows).

Table S1 Average grain size (AGS) and breakdown strength (E_b) of all ceramics.

x (mol%)	0	0.05	0.10	0.15	0.20	BMT15-RRP	BMT20-RRP
AGS (μm)	3.43	2.04	1.47	1.04	1.36	0.31	0.54
E_b (kV·cm^{-1})	300	380	420	470	440	560	498

On the one hand, the relationship between the breakdown strength (E_b) and AGS can be summarized as $E_b \propto 1/\sqrt{AGS}$, that is, reducing the average grain size of ceramics is beneficial to the increase of E_b value. On the other hand, in dielectric ceramics, depletion regions generated by the grain boundaries can prevent charge carriers from passing through them. The density of grain boundaries increases with the decrease of grain size, resulting in more depletion regions, higher resistivity and larger E_b, that is, grain refinement can improve E_b. In fact, in this study, the breakdown strength of the dielectric material does decrease with the reduction of the ceramic grain size, which will be confirmed later.

Experimental

Phase-Field Simulations: A single crystal considering Cubic (*C)* to Tetragonal (*T*) to rhombohedral (*R*) ferroelectric transition with defect doping concentration *x*=0-0.20 has been carried out in phase-field simulations. The total free energy of the ferroelectric system can be described as:[1-4]

$$F = \int_V (f_{bulk} + f_{grad} + f_{couple})\, dV + \int_V (f_{elas} + f_{elec}) dV \quad (1)$$

where f_{bulk} represents the bulk free energy density,

$$f_{bulk} = \alpha_1(P_1^2 + P_2^2 + P_3^2) - \alpha_{11}(P_1^2 + P_2^2 + P_3^2)^2 + \alpha_{12}(P_1^2P_2^2 + P_2^2P_3^2 + P_1^2P_3^2)$$

$$+\alpha_{112}(P_1^4P_2^2 + P_2^4P_3^2 + P_1^4P_3^2 + P_1^2P_2^4 + P_2^2P_3^4 + P_1^2P_3^4) + \alpha_{113}(P_1^2P_2^2P_3^2)$$

$$+\alpha_{111}(P_1^2 + P_2^2 + P_3^2)^3 \quad (2)$$

where α_{ij} is the coefficient and depends on concentration c and temperature T.

f_{grad} represents the gradient energy density,

$$f_{gradient} = \frac{1}{2}G_{11}[(P_{1,1})^2 + (P_{1,2})^2 + (P_{1,3})^2 + (P_{2,1})^2 + (P_{2,2})^2 + (P_{2,3})^2 + (P_{3,1})^2 + (P_{3,2})^2 + (P_{3,3})^2] \quad (3)$$

where G_{11} is the gradient energy coefficient. f_{couple} represents the dipole effect caused by doping.

$f_{\text{couple}} = -\int d^3x \sum_{i=1,2,3} P_i(x) \cdot \varphi_{loc}(x)$, where $\varphi_{loc}(x)$ is dipolar field created by doping, and is assumed to distribute randomly and doesn't change under cooling. f_{elas} is the long-range elastic interaction energy densities and f_{elec} is the electrostatic interaction energy densities. $f_{elas} = \frac{1}{2}c_{ijkl}e_{ij}e_{kl} = \frac{1}{2}c_{ijkl}(\varepsilon_{ij} - \varepsilon_{ij}^0)(\varepsilon_{kl} - \varepsilon_{kl}^0)$, where c_{ijkl} is the elastic constant tensor, ε_{ij} the total strain, ε^0_{kl} the electrostrictive stress-free strain, i.e., $\varepsilon^0_{kl} = Q_{ijkl}P_kP_l$. $f_{elec}=f_{dipole}+f_{depola}+f_{appl,}$ where f_{dipole} is the dipole-dipole interaction caused by polarization, f_{depola} the depolarization energy density and f_{appl} the energy density caused by applied electric field. The temporal evolution of the spontaneous polarization field (P) can be obtained by solving the time-dependent Ginzburg-Landau (TDGL) equation:$\frac{dP_i(x,t)}{dt} = -M\frac{\delta F}{\delta P_i(X,t)}$, i=1, 2, 3, where M is the kinetic coefficient, F is the total free energy, and t is time.

References

1 S. Semenovskaya and A. G. Khachaturyan, *J. Appl. Phys.*, 1998, **83**, 5125-5136.

2 D. Wang, X. Ke, Y. Wang, J. Gao, Y. Wang, L. Zhang, S. Yang and X. Ren, *Phys. Rev. B*, 2012, **86**, 054120.

3 Y. L. Li, L. E. Cross and L. Q. Chen, *J. Appl. Phys.*, 2005, **98**, 064101.

4 L. Zhang, X. Lou, D. Wang, Y. Zhou, Y. Yang, M. Kuball, M. A. Carpenter and X. Ren, *Phys. Rev. Appl.*, 2017, **8**, 054018.